Comparative study of vinylene carbonate and lithium difluoro(oxalate)borate additives in a SiO_x/graphite anode lithium ion battery in the presence of fluoroethylene carbonate

Xiaozhou Huang,[1] John Shea,[1,2] Junxiang Liu,[1] Nader Marandian Hagh,[3] Shubha Nageswaran,[3] Jing Wang,[1] Xianyang Wu,[1] Gihan Kwon,[4] Seoung-Bum Son,[1] Tongchao Liu,[1] Jihyeon Gim,[1] Chi-Cheung Su[1], Pei Dong,[2] Chengcheng Fang,[5] Matthew Li,[1,*] Khalil Amine,[1,*] Umamaheswari Jankairaman[3,*]

[1]Chemical Sciences and Engineering Division, Argonne National Laboratory, Lemont, Illinois 60439, United States of America

[2]Department of Mechanical Engineering, George Mason University, Fairfax, Virginia 22030, United States of America

[3]Advanced Battery Cell Engineering, General Motors, Warren, Michigan 48093, United States of America

[4]National Synchrotron Light Source II, Brookhaven National Laboratory, Upton, New York 11973, United States of America.

[5]Department of Chemical Engineering and Materials Science, Michigan State University, East Lansing, MI 48824, USA

Corresponding Author: matthew.li@anl.gov, amine@anl.gov, uma.viswanathan@gm.com

Keywords: Silicon oxide anode, Vinylene carbonate, Lithium difluoro(oxalate)borate, Fluoroethylene carbonate, Solid electrolyte interface

Abstract

The SiO_x/graphite composite is recognized as a promising anode material for lithium-ion batteries (LIBs), owing to the high theoretical capacity of SiO_x combined with the excellent stability of graphite. However, the inherent disadvantage of volume expansion in silicon-based anodes places significant challenges on the solid-electrolyte interphase (SEI) and severely degrades the electrochemical performance. Rational formulation of electrolyte, including its additives, is crucial in accommodating and optimizing the composition of the SEI and enhancing cell performance. In this work, we present a comparative study of vinylene carbonate (VC) and lithium difluoro(oxalate)borate (LiDFOB) additives combined with fluoroethylene carbonate (FEC) in the electrolyte for SiO_x/graphite||$LiNi_{1-x-y-z}Co_xMn_yAl_zO_2$ full cells. VC outperformed LiDFOB as an additive, delivering higher capacity cycling, higher coulombic efficiency and better cycle stability up to 400 cycles. XPS and impedance analysis reveals that LiDFOB contributed to SEI/CEI with both a lower proportions of LiF and a higher proportions of poly(VC), which tended to produce higher cell impedance. XRD and XANES further indicated that using the LiDFOB additive the NCMA cycled to a shallower degree than that of the VC additive. Although the VC-additive maintained a higher capacity up to 400 cycles, microstrain and SEM analysis shows a higher strained NCMA along with clear evidence of cracking over the surface of the NCMA particle in VC-based electrolyte but not in LiDFOB. This suggests that the negative influence of LiDFOB at the anode (inferior SEI) supersedes the negative impact of both a cracked NCMA and a deeper cycled NCMA and SiO_x-based anode.

Introduction

Lithium-ion batteries (LIBs) have emerged as one of the most important rechargeable batteries in a variety of fields, such as consumer electronics, electric vehicles, and energy storage devices. Despite their widespread use, the advancement of LIB technology encounters a bottleneck due to the low theoretical capacity of conventional graphite anodes (372 mAh/g).[1-6] Silicon, boasting an exceptionally high theoretical capacity of 3579 mAh/g ($Li_{15}Si_4$), attracting increasing attention as a promising alternative anode material for LIBs.[7-12] However, silicon's substantial volume expansion during cycle processes poses significant challenges, including particle fragmentation, material detachment, and instability of the solid electrolyte interface (SEI), hindering battery longevity and safety. In contrast, silicon oxide (SiO_x, where $0 < x < 2$) emerges as a compelling substitute for silicon, attributed to its cost-effectiveness and reduced volume variation.[13] Notably, during initial lithiation, the formation of lithium silicate compounds such as Li_4SiO_4 and $Li_2Si_2O_5$, along with lithium oxide (Li_2O), effectively mitigate SiO_x's volume fluctuations, ensuring robust cycling stability.[14] The use of SiO_x/graphite composite anode can further reduce volume expansion, improve stability, and enhance conductivity of the anode.

To enhance the cycling stability of SiO_x-based LIBs and reduce SEI failure caused by volume expansion, numerous additives have been explored. For example, fluoroethylene carbonate (FEC) has shown promise as an additive for silicon anode LIB,[15-17] because it can generate a stable SEI rich in LiF and polymer, which is believed to be beneficial for accommodating the volume changes inherent in silicon-based anode during cycling.[18] Nevertheless, high concentration of FEC can lead to increased generation of hydrofluoric acid (HF) during cycling at elevated temperatures, which promote transition metal dissolution from the

cathode.[19] When used at additive levels, the cycle stabilizing effect of FEC is eventually reduced as it is gradually consumed over the course of cycling.[18]

Vinylene carbonate (VC) is an effective commercialized additive for silicon-based anode LIB.[17] It has been reported that VC could generate a reasonably stable SEI on the surface of Si@SiO_x/C composite anode.[20] Akin to FEC, SEI formed in VC electrolyte contains cross-linked poly(ethylene oxide) and aliphatic chain functionalities with carbonate and carboxylate functional groups.[21] The SEI, enhanced by these organic and inorganic compounds, demonstrates improved resilience against the volume expansion of silicon-based anodes. VC is also known for its ability to stabilize graphite materials on the anode, which is beneficial for improving the compatibility of SiO_x/graphite composite anode. Alternatively, lithium difluoro(oxalate) borate (LiDFOB) serves as another common electrolyte additive that can produce a thinner and LiF-rich SEI to extend the cycle life of graphite and silicon anodes.[22, 23] It has been observed that FEC alone fails to establish a stable film on graphite surfaces, but the addition of LiDFOB has been shown to address this issue.[24] This suggests that LiDFOB may serve as a suitable additive to improve the stability of SiO_x/graphite composite anodes in LIB.

Although VC and LiDFOB each have their advantages, comparative studies of their use in combination with the FEC additive in a standard 1M $LiPF_6$ EC/EMC (3:7 volume ratio) electrolyte with a SiO_x/graphite composite anode are seldom reported. In this study, we conduct a comprehensive analysis of the effects of VC and LiDFOB additives on cycling performance. Additionally, we delve into the mechanisms underlying these effects by employing scanning electron microscopy (SEM), X-ray Diffraction (XRD), X-ray absorption spectroscopy (XAS), X-ray photoelectron spectroscopy (XPS), and Electrochemical impedance spectroscopy (EIS).

Experimental

Materials:

The electrolyte consisted of 1M $LiPF_6$ in a mixture of ethylene carbonate (EC) and ethylmethyl carbonate (EMC) at a volume ratio of 3:7, supplemented with an additional 2 wt% of fluoroethylene carbonate (FEC) and either 1 wt% of vinylene carbonate (VC) or lithium difluoro(oxalato)borate (LiDFOB).

Electrochemical Characterization:

To prepare NCMA cathode $LiNi_{1-x-y-z}Co_xMn_yAl_zO_2$ where (x, y, z <1), 1.5% of Super P was dispersed in PVDF-NMP solution with total PVDF content of 1.4%. CNT solution with 0.1% of CNT was then added to the mixture. 97% active NCMA was added at the final stage. The loading density of NCMA cathode was ~3.0 mAh/cm^2. For the SiO_x/graphite anode (where 1 < x <2, 95 wt% of SiO_x/Graphite was mixed with 2% of styrene-butadiene rubber (SBR)/ 2% sodium carboxymethyl cellulose (CMC) and 1% carbon black. The loading density of the SiO_x anode was 3.4 mAh/cm^2.

The 2032 coin full-cells were assembled using a 14-mm NCMA cathode, a 15-mm SiO_x/graphite anode, Entek Ceramic-Coated separator, and 60 µL of LiDFOB or VC electrolyte in an argon filled glove box. All cells were crimped by an automatic coin cell crimper purchased from Hohsen Corp. All electrochemical measurements were taken on a NEWARE cycler. For the cycling experiments, each cell was taken the initial formation under the following conditions: constant

current charging at 0.238 mA (C/10), constant voltage charging at 4.2 V with a cutoff current of 0.024 mA, and constant current discharging at 0.238 mA (C/10) for three cycles. Subsequently, all cells were subjected to cycling under a constant current charge of 1.59 mA (C/3), constant voltage charge at 4.2 V with a cutoff current of 0.238 mA, and constant current discharge at 1.59 mA (C/3). The cycle tests ended at 400th cycle.

The EIS of the cells was measured using an electrochemical workstation from Solartron Analytical (1470E Cell Test System), with a scanning frequency range from 0.1 Hz to 100,000 Hz. The EIS of each cell was performed after the formation cycles.

Physical Characterization:

The surface morphology of cathode and anode samples were characterized by a scanning electron microscopy (SEM, JEOL IT800HL). The surface composition was characterized by XPS technique using a Physical Electronics PHI 5000 VersaProbe II system photoelectron spectrometer at an operating pressure of 1×10^{-7} Torr. The XPS samples were taken from full cells after they were subjected to the formation and 10 cycles. The samples were rinsed gently with DMC. XPS was conducted by directly transferring electrodes from glovebox into the XPS equipment without exposure to air.

The surface compositions were characterized by the operando synchrotron X-ray diffraction (XRD) that were conducted at the beamline 28-ID-1 of Brookhaven National Laboratory with a wavelength of 0.1665 Å. The synchrotron instrument parameters were calibrated by the CeO_2 standard. X-ray absorption spectroscopy (XAS) experiments for the NCMA cathode were carried out at 7-BM-B beamline of National Synchrotron Light Source II (NSLS-II) of Brookhaven National Laboratory. The synchrotron instrument parameters were calibrated by the CeO_2 standard.[25]

Results and Discussion

Cycling performance of NCMA cathode and SiO_x/graphite composite anode full cell

The capacity retention and coulombic efficiency (CE) for cells with two different electrolytes containing 1 wt% of LiDFOB and VC additives, respectively, are plotted in **Figure 1**. The first three cycles are formation cycles that operate at C/10 (**Figure 1a**), followed by cycling at C/3 (**Figure 1b**). During the formation process, the first cycle of LiDFOB produced a higher discharge capacity than that of VC whereupon, VC began to yield a higher capacity than LiDFOB from the 2nd cycle. The initial CE of VC is 82.78%, slightly lower than the 83.51% of LiDFOB. This indicates that the cell with VC as an additive consumed slightly more Li^+ ions compared to the LiDFOB cell to form the SEI. The subsequent formation cycles show the VC-based electrolyte producing a higher discharge capacity than that of LiDFOB (2.89 mAh cm^{-2} vs 2.83 mAh cm^{-2} at the third formation cycle). The same trend is observed as post formation with VC maintaining a higher discharge capacity.

The areal capacity of cells with VC additive was found to be consistently larger than that of LiDFOB (Figure 1b). After normalizing the discharge capacity to the first cycle after the formation process (**Figure 1c**), the same trend is maintained. At ~250 cycles, the performance of LiDFOB began to deteriorate at a significantly quicker rate. This was also accompanied with a sudden drop in coulombic efficiency. LiDFOB has been previously shown to perform quite well

for Si-based anodes[26] and NMC-based cathodes.[26] However, the capacity retention results suggest that this ability is not consistently maintained throughout the cycling process and not as long-lasting as VC. At the end of test, the capacity retention was 77% for VC electrolyte and ~72% for LiDFOB electrolyte relative to 1st cycle post formation. The cycling results reveal that the VC additive demonstrates a consistently higher specific capacity than the LiDFOB additive throughout the entire cycling process.

The voltage profiles at various cycles can be found in **Figure 1d** along with the $dQdV^{-1}$ for various cycles from **Figure 1e-h**. During the first formation cycle, the charging peaks from 3.5-3.75 V shifted to a higher potential for the LiDFOB-containing cells when compared to the VC-containing electrolyte. As no significant difference in peak positions were found at other SOCs and on the subsequent discharge, the observed difference of the first charge peaks (from 3.5-3.7 V) likely stems from differing SEI/CEI formation potentials. Post formation and at the 10th cycles, the difference was very minor with LiDFOB exhibiting a slight shift in all peak position, indicating a slightly higher impedance. One key feature of interest is that at the 400th cycles, the upper voltage plateau (~4.0 V) of the LiDFOB-containing cell appears to be higher than that of the VC-containing cell (~3.9 V). This is reflected more clearly in the $dQdV^{-1}$ of the data (**Figure 1e-h**). At the 400th cycle, the same clear lower voltage shift of the ~4.0 V peak to ~3.9 V is observed (Figure 1h) . Moreover, it appears the entire impedance of the cell using VC is larger than that of LiDFOB, yielding a shift in all $dQdV^{-1}$ peaks to a higher/lower potential during charge/discharge, respectively. Interestingly, the reduction peak at ~3.9 V of VC is much larger in magnitude than that of LiDFOB. The reason for the larger capacity of VC over LiDFOB in this voltage regime when the potential is lower for VC remains to be seen.

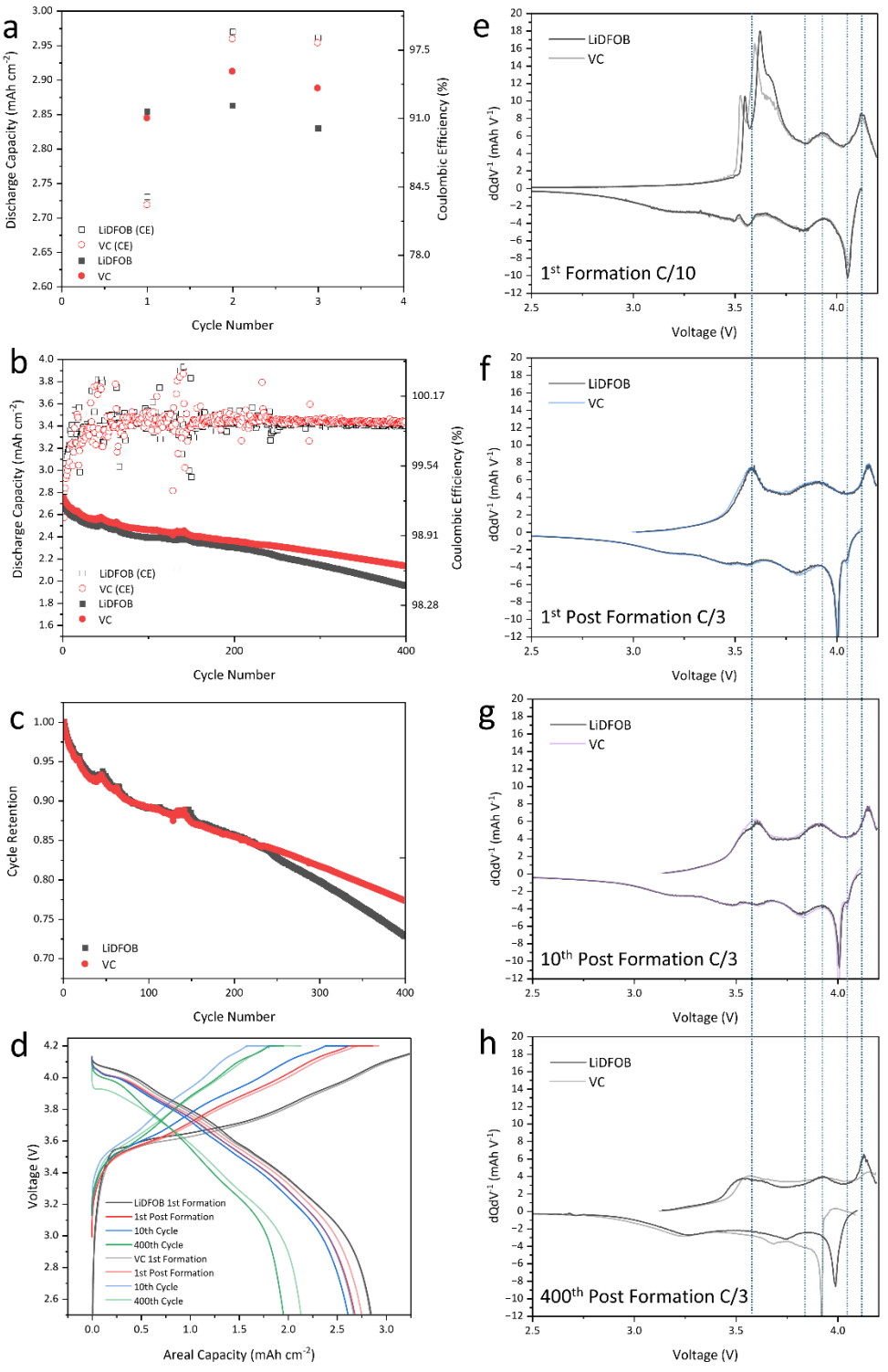

Figure 1. Cycle performance of cells with 1 wt% of LiDFOB and VC additives in the electrolyte for silicon-anode LIB. Specific capacity changes with cycle number for a) formation process and

b) cycle process. c) Capacity retention normalized to 1st cycle post formation. d) Voltage profile at various cycles, e-h) dQ dV^{-1} from 1st formation cycle, 1st cycle post formation, 10th cycle post formation, and 400th cycle post formation, respectively.

SEM analysis for NCMA cathode and SiO_x/graphite composite anode

In an attempt to investigate the cause of the differences in performance, the morphology of the cathode and anode was investigated. SEM was performed on cathode and anode harvested from coin cells at different cycle numbers. As expected, there are no discernable differences in morphology between the pristine (**Figure S1**) and NCMA cycled in LiDFOB or VC-based electrolytes directly after formation and at the 10th cycle (**Figure S2 a-d**). This aligns well with the cycling results. However, at the EOT (400 cycles), we observed a degree of void formation/cracking on the surface of the NCMA particles cycled with VC (**Figure S2**e) whereas the one cycled with LiDFOB did not have any apparent changes beside some debris accumulation. This is inconsistent with the poorer cycle retention of LiDFOB than VC, possibly indicating that perhaps the anode is the cause of the poorer performance for LiDFOB rather than the cathode. However, this could explain the larger impedance from $dQdV^{-1}$ of the VC sample. As the NCMA particles crack, more electrochemically active surface area is introduced to the cell. While this might temporarily decrease the impedance for the immediate cycles post cracking, the buildup of additional and substantial amount of CEI likely resulted in the observed higher impedance.

Looking at the anode, the SEM of the SiO_x/graphite electrode's morphology at different cycle numbers for both electrolytes are shown in **Figure 2**. The SEM and EDS mapping of pristine SiO_x/graphite particle are shown in **Figure 2a** and **Figure 2b,** respectively. Differentiation between the graphite and Si-based material can be easily made based on the EDS mapping. After formation process, the SiO_x particles show very little degradation **Figure 2c** and **Figure 2d** in both electrolytes**.** The SiO_x particles are degraded in both VC and LiDFOB electrolyte. It is evident that the anode employing the LiDFOB-containing electrolyte retains its structure better than that of the VC electrolyte, showing less fracture in LiDFOB up to 10 cycles (**Figure 2e** and **Figure 2f**). One possible explanation is that the lower degree of lithiation of the SiO_x/graphite anode in the LiDFOB-based electrolyte induced less volume expansion in comparison to the VC-containing electrolyte. This would produce a less cracked SiO_x and NCMA. However, this effect was not found at the end of the test. In fact, the anode cycled with LiDFOB-based electrolyte exhibited arguably more signs of pulverization (**Figure 2h**) than the one cycled with VC (**Figure 2g**). Moreover, there is clearly a larger interparticle pore volume for the cell cycled with VC over LiDFOB-containing electrolyte. It is likely that the pores that are supposed to be present for the LiDFOB-containing electrolyte is actually filled with an excessive buildup of SEI at the end of test, which aligns well with the lower CE of LiDFOB-containing electrolyte and higher rate of cycle degradation.

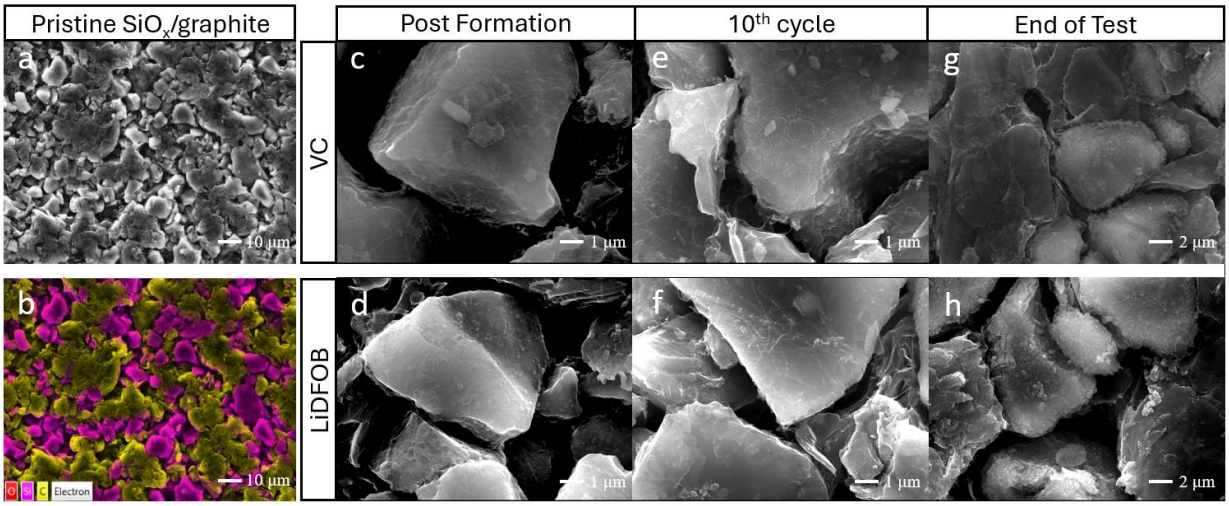

Figure 2. SEM images for SiO_x/graphite composite anode for pristine (a) SEM and (b) EDS, post formation (c-d), 10th cycle (e-f), and end of test (g-h) in VC and LiDFOB electrolyte.

XPS analysis for NCMA cathode and SiO_x/graphite composite anode

Given the significant impact of the SEI/CEI on cycling, XPS was utilized to examine the surface composition of SiO_x/graphite composite anodes and NCMA cathodes from cells containing either LiDFOB or VC containing electrolytes after 10 cycles. Briefly, the C1s peaks (are deconvoluted into seven components with the adventitious C=C sp^2 at 284.8 eV, including C–C (285.6 eV), C–O (286.5 eV), C=O (287.8 eV), CO_3^{2-} (289.0 eV), poly(VC) (290.3 eV), PVDF (291.4 eV), and Li_xC_6 (283.0 eV).[27-29] Li_xC_6 only exists on anode. The C1s peak on cathode at around 291.4 eV are mainly attributed to PVDF binder and exclusively to poly(VC) for the anode as PVDF was not used as the binder. The F1s peaks are deconvoluted into two components, including LiF (685.0 eV) and a combination of P-F, B-F and C-F bonds (686.7-687.4 eV), which was not attempted to be further deconvoluted.[17,30] The P-F bond is from $Li_xPF_yO_z$, a typical compound in SEI. The B-F and C-F bonds are attributed to LiDFOB and FEC, respectively. The O1s peaks are deconvoluted into three components, including C=O (532.0 eV), C-O (533.5 eV), RO-Li (330.0-330.5 eV) and Metal-O (529.0 eV).[28, 30] RO-Li is from some side reactions between Li and solvent.[30] Metal-O bond only exist on cathode surface. No significant difference between VC and LiDFOB can be differentiated using the Li 1s (**Figure S3**). Si 2p (**Figure S4**) reveals a slightly larger Si signal in the LiDFOB-containing electrolyte. The atomic composition of various element as analyzed by XPS is presented in **Table S1**.

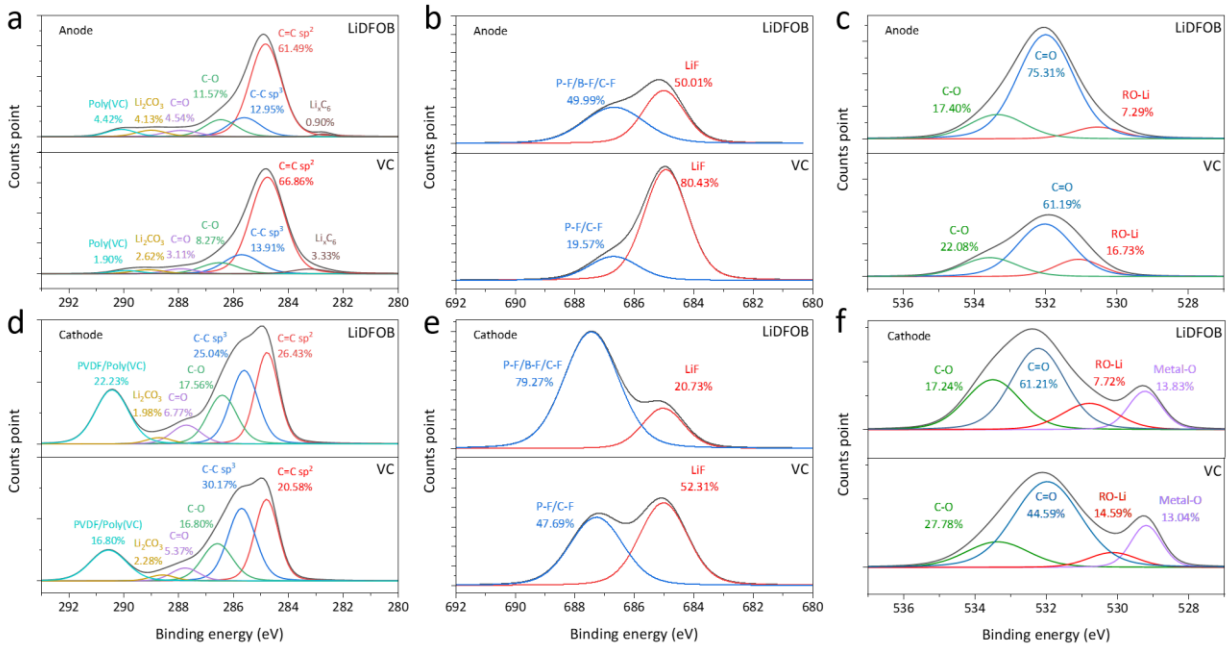

Figure 3. C1s, F1s, and O1s for SiO_x/graphite composite anode and NCMA cathode that were cycled 10 times after formation in LiDFOB or VC electrolyte, (a-c) anode and (d-f) cathode.

The F 1s peak from 686.7 to 687.3 eV was found to be higher in LiDFOB than in VC (**Figure 3b** and **Figure 3e**), likely due to the contribution of the B-F bond from LiDFOB in addition to the typically present P-F bond. B-F/P-F are much too convoluted to drawn reliable conclusions. Perhaps the more informative peak is that of LiF centered at ~685 eV. Although both electrolytes contain FEC (main source of LiF), the addition of another source of LiF (LiDFOB) would be expected to promote the formation of comparatively more LiF. Surprisingly, this was found to be not the case. Upon deconvoluting the contribution of P-F/B-F/C-F and LiF, the LiF concentration in the SEI derived from the LiDFOB electrolyte is much lower than that in the VC electrolyte (Figure 3b and Figure 3e), even when taking F atomic concentration into consideration (Table S1). This result aligns with another study which found that the SEI generated with a LiDFOB additive in a FEC-based electrolyte contained less LiF compared to an SEI formed without the LiDFOB additive.[24] We believe this is related to the tendency of LiDFOB to form nanosized LiF.[31] Specifically, the formation mechanism of LiF stems from the propensity of LiDFOB's oxalate moiety to bind to LiF (capping effect). This has been shown to promote the formation of a thin organic layer over the surface of nanostructured LiF as illustrated in a TEM study by Jurng et al.[31] Supporting this, we also observed a higher concentration of C-O and C=O bonds in C1s and O1s in the LiDFOB electrolyte (**Figure 3 a** and **c**) compared to that in the VC electrolyte, presumably from the carboxylate layer formed from LiDFOB. The role of the capping layer is not clear but it appears to hinder LiF formation. Interestingly, the concentration of poly(VC) is higher in the LiDFOB electrolyte than in the VC electrolyte on both the anode and cathode from C1s (**Figure 3a and Figure 3d**). This is surprising as VC is expected to form poly(VC) while LiDFOB is not. For the anode, we suspect that this might be related again to the tendency of LiDFOB to produce nanostructured LiF.[31] Although nanostructured LiF have been previously argued to produce more uniform diffusion fields, benefiting Li metal plating,[31] is impact on SiO_x anodes are less clear.

As the reduction potential of FEC is higher than that of VC (due to the fluorine atom), it should be the main poly(VC) forming agent, in the absence of LiDFOB, the decomposition of FEC likely promoted larger-sized LiF. While it is unknown why the smaller sized LiF seem to trigger more poly(VC) formation, we can speculate. It is possible that the LiF formed in LiDFOB-containing electrolytes are not only smaller in dimension but also lesser in total mass of LiF, offering less total surface coverage of the anode. If this is the case, the nano-sized LiF are less effective in passivating the anode and therefore demands more poly(VC) to achieve passivation of the anode. Unfortunately, more poly(VC) without the presence of a high amount of LiF, has been shown to yield a higher impedance.[32-34] Similar XPS trends were observed for the CEI (**Figure 3d-f**). Finally, the use of LiDFOB is known to form a surface layer that can be used for passivating the cathode's surface against oxidation.[35] Together, both the CEI/SEI may impart measurable impedance, which aligns well with the 10^{th} post-formation cycle $dQdV^{-1}$ (Figure 1f and g) and also electrochemical impedance spectroscopy after the 1^{st} post-formation cycle (Figure S5).

The reason for the lower coulombic efficiency and poorer cycle retention is likely related to the nature of the SEI. XPS of Si 2p of the anode cycled LiDFOB-containing electrolyte had a slightly stronger Si signal over VC-containing electrolyte. This suggests either that the LiDFOB-based SEI is either thinner (<penetration depth of XPS) or more porous than VC's SEI. Given that the impedance is higher in the LiDFOB-based cells in addition to the fact that the Si anode appeared more porous from the 400^{th} cycle SEM (discharged state), the SEI based on LiDFOB additive is unlikely to be the cause. Accordingly, it is more likely that the XPS of Si 2p indicates a higher SEI porosity, allowing more excited electrons to escape the sample to reach the detector. A study by Zhang *et al* indicated that porous SEI will have its pores enlarged upon lithiation of Si-based anode due to tensile stress. This will increase the diffusion coefficient of electrolyte constituents in the SEI phase which accelerates the formation of new SEI.[36] When taken together, these results suggest that the cause of the poor cycle retention and lower coulombic efficiency in the LiDFOB-additive stems from the anode.

XRD and XANES analyses on NCMA cathode

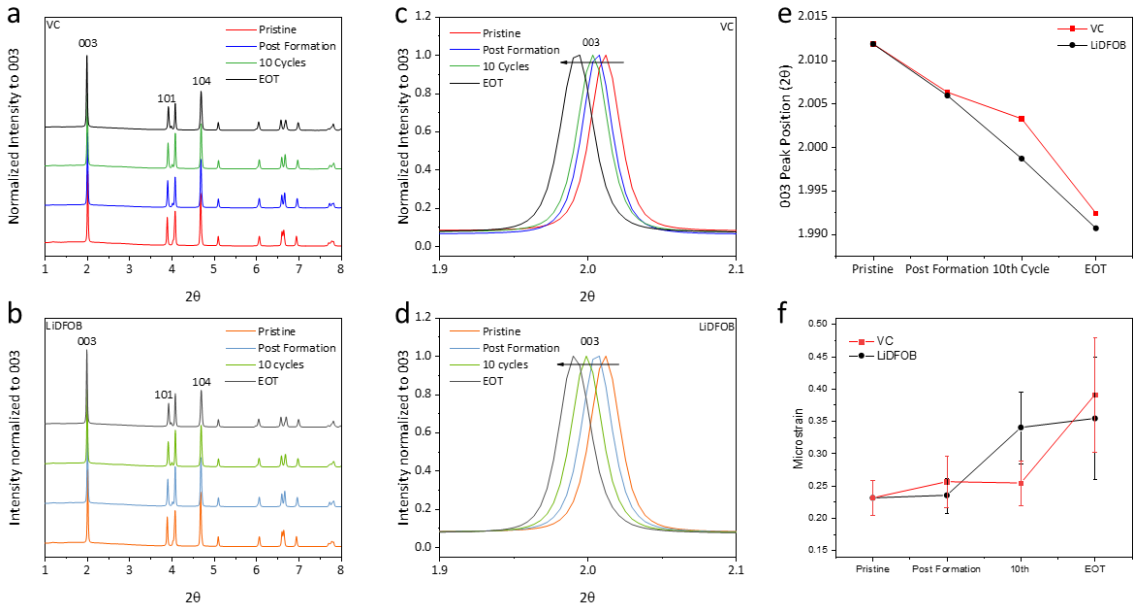

Figure 4. XRD analysis for NCMA cathode at different cycle with LiDFOB or VC additives. (a) and (b) XRD spectra for NCMA cathode cycled in VC electrolyte harvested at the discharged state; (c) and (d) peak (003) of NCMA cathode cycled in VC electrolyte; (e) Comparison of 2θ changes for NCMA cathode cycled in VC or LiDFOB electrolyte; (f) Comparison of microstrain changes for NCMA cathode cycled in VC or LiDFOB electrolyte.

This conclusion is also reflected in further characterization of the NCMA cathode. The negative implication of LiDFOB-derived SEI/CEI is also reflected in the NMC material. To evaluate the impact of additives on structure of NCMA cathode, XRD was performed at different cycle numbers: pristine, post-formation, 10th cycle samples, and EOT (**Figure 4a and 4b**). It is shown that the (003) shifts toward lower 2-theta for both LiDFOB and VC as the cell is cycled with LiDFOB exhibiting a more significant shift than VC (**Figure 4c-e**). This indicates there is a greater increase in $d_{(003)}$ spacing and more lattice expansion along the c-axis. While the shift was generally more drastic for LiDFOB than VC-containing electrolyte, the 10th cycle exhibited the largest difference in the (003) peak position between LiDFOB and VC. As the c-axis spacing closely tracks the degree of Li-ion content in the cathode,[37] this suggests that the NCMA cycled with LiDFOB has a lower ability to lithiate than that of VC. A similar but less drastic finding can be seen for the EOT samples. This agrees with the cycle performance where the LiDFOB additive results in a consistently lower specific capacity and coulombic efficiency during the entire cycling, which likely stems from a quicker Li-ion consumption at the anode. A similar trend is also supported by XANES (X-ray absorption near edge spectroscopy). XANES performed at the Ni, Co, and Mn K-edge on NCMA cathode harvested from at post formation and the 10th cycle is shown in **Figure 5a-c**, respectively. Compared with the pristine NCMA, both LiDFOB and VC-based electrolyte produced NCMA with more oxidized Ni and Co. A higher oxidation state implies an inability of the NCMA to be lithiated during discharge i.e. less discharge capacity. The LiDFOB-containing electrolyte produced Ni and Co with comparatively higher oxidation state than VC-

containing electrolyte for both the post formation and 10th cycle. This is consistent with the XRD results where LiDFOB yielded the largest shift of the (003) peak (Figure 4e).

Interestingly, we found that FWHM$_{hkl}$ of the VC-based cathode was smaller than that of LiDFOB after 10 cycles (**Figure 4f**). Estimation of microstrain by the Williamson-Hall analysis (**Figure S6**)[38] indicates that the microstrain of NCMA cycled in the two electrolyte were similar and within error except for the 10th cycle where the separation was clearly large. The 10th cycle was also where difference in the (003) peak position was the largest. It is somewhat unexpected that the LiDFOB-containing electrolyte produced an NCMA with a higher microstrain because the lower capacity cycling in LiDFOB-containing electrolyte (presumably induced by the anode) will likely result in a NCMA that is cycled to a shallower degree. The fact that the microstrain is higher for the LiDFOB-containing electrolyte indicates that the lower capacity of LiDFOB-based electrolyte is not only related to the impedance imparted by differing CEI/SEI composition, but also likely stemming from some structural differences i.e. LiDFOB induces some damage that is not present in VC.

However, at EOT, the microstrain of VC-based electrolyte increased while that of LiDFOB-based electrolyte did not significantly change from the 10th cycle to EOT. The microstrain of VC does appear to be slightly larger than LiDFOB (although it is within error). When looking at the post cycling SEM, Figure S2), there are clear indications of cracks over the surface of the NCMA cycled in VC-based electrolyte (Figure S2e), while no cracks can be seen when cycled with the LiDFOB-based electrolyte (Figure S2f). This points to the microstrain of NCMA cycled in VC-based electrolyte to be higher at EOT. The cause of the cracking is likely due to a deeper capacity discharge, using more of the NCMA's capacity and causing more volume expansion/contraction over cycling. However, since the capacity of the VC-containing cell is still larger than that of the LiDFOB-containing cell at EOT, it seems that the negative impact of LiDFOB on the anode supersedes negative performance effects due to structural damage of the cathode.

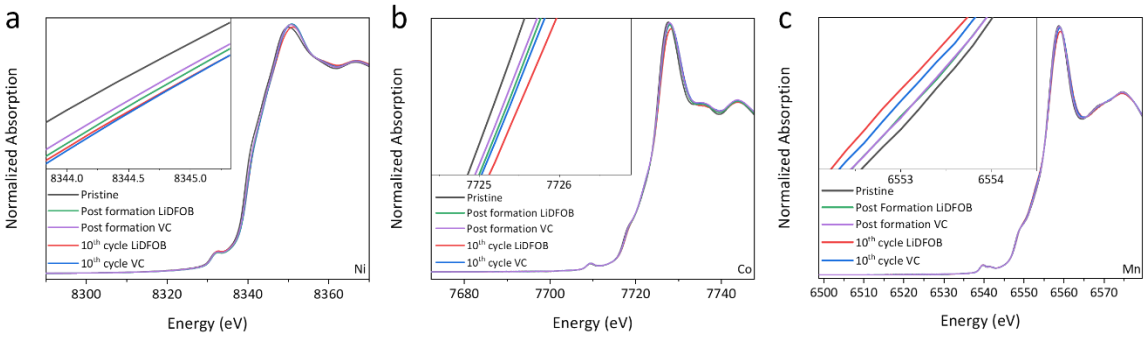

Figure 5. XANES analysis for NCMA cathode at the discharged state harvested at different cycle status with LiDFOB or VC additives. a) Ni K-edge, b) Co K-edge, and c) Mn K-edge.

Conclusions

A comparative study was performed on NCMA/SiO_x+graphite full cells (coin cells) using 1M $LiPF_6$ in EC/EMC at a volume ratio of 3:7, with 2 wt% of fluoroethylene carbonate (FEC) and either 1 wt% of vinylene carbonate (VC) or lithium difluoro(oxalato)borate (LiDFOB). The cells containing VC significantly outperformed those containing LiDFOB, in terms of delivering a higher discharge capacity, higher coulombic efficiency during cycling, and along with a higher cycle retention of ~77% vs 72 %. Interestingly, LiDFOB produced a higher coulombic efficiency and capacity only during the first formation cycles at C/10. However, upon switching to the cycling current of C/3, the performance of VC immediately began to exhibit both higher coulombic efficiency and capacity. Analysis of SEI composition *via* XPS, revealing both the CEI and SEI of the LiDFOB-containing cells contained less LiF and more poly(VC). When taken together with a higher full cell impedance after formation for LiDFOB, it appears that the use of LiDFOB imparted the cell with an organic-based SEI/CEI layer that are typically considered more impedance inducing. XPS at Si 2p of cycled anodes indicated a stronger Si signal with LiDFOB additive, which points to a more porous and less passivating SEI. SEM analysis of the anode harvested after the 400^{th} cycle further revealed much more interparticle pore volume in the anode cycled with LiDFOB, suggesting more volume expansion. At the cathode, clear signs of NCMA cracking at the 400^{th} cycle can be found only for the VC-containing electrolyte, which does not correspond to the observed higher performance of the VC-based system. This was also supported by a higher 400^{th} cycle microstrain (albeit with overlapping error bars) for the VC additive. XRD and XANES analysis both show that NCMA cycled in LiDFOB-containing electrolyte can re-lithiate to a lesser extent than the VC-containing electrolyte, aligning nicely with a lower capacity cycling. It appears that even with a cracked NCMA cathode at the 400^{th} cycle in addition to a higher usage of NCMA and SiO_x specific capacities, the VC sample can still outperform the LiDFOB additive. The inability of LiDFOB in protecting the Si-based anode relative to VC likely controlled the performance of the cell. While our study focuses on the electrochemical performance of LiDFOB, it is known that LiDFOB can generate gas under certain conditions, which may not be evident in coin cell studies. Future research with methods to detect gas generation could offer more insights.

Supporting Information

The supporting information is available, including additional supporting Figures and Table.

Acknowledgement

The authors would like to acknowledge support from General Motors Inc. and the US Department of Energy (DOE), Office of Energy Efficiency and Renewable Energy, Vehicle Technologies Office. Argonne National Laboratory is operated by the DOE Office of Science by UChicago Argonne, LLC, under contract number DE-AC02–06CH11357. Work performed (Scanning electron microscopy) at the Center for Nanoscale Materials, a U.S. Department of Energy Office of Science User Facility, is supported by the U.S. DOE, Office of Basic Energy Sciences, under Contract No. DE-AC02–06CH11357. Use of the National Synchrotron Light Source II (beamline 7-BM and 28-ID-1) is supported by the US Department of Energy, an Office of Science user Facility operated by Brookhaven National Laboratory under contract number DE-SC0012704. The authors would like to acknowledge the use of ChatGPT 3.5 by OpenAI for

general grammar and language review of manuscript. The authors would like to express our gratitude to General Motors for their generous financial support.

References

(1) Blomgren, G. E. The Development and Future of Lithium Ion Batteries. *Journal of The Electrochemical Society* **2017**, *164* (1), A5019. DOI: 10.1149/2.0251701jes.
(2) Xie, Y.; Li, J.; Li, M.; Cai, J.; Huang, X.; Nguyen, H.; Yu, L.; Huo, D.; Yang, Z.; Karami, N.; et al. Modifying Surface Chemistry to Enhance the Electrochemical Stability of Nickel-Rich Cathode Materials. *Advanced Functional Materials* **2024**, *34* (14), 2311551. DOI: https://doi.org/10.1002/adfm.202311551 (acccessed 2024/05/06).
(3) Wong, H.; Liu, T.; Tamtaji, M.; Huang, X.; Tang, T. W.; Hossain, M. D.; Wang, J.; Cai, Y.; Liu, Z.; Liu, H.; et al. Graphene-supported Single Atom Catalysts for High Performance Lithium-oxygen Batteries. *Nano Energy* **2024**, *121*, 109279. DOI: https://doi.org/10.1016/j.nanoen.2024.109279.
(4) Manthiram, A. An Outlook on Lithium Ion Battery Technology. *ACS Central Science* **2017**, *3* (10), 1063-1069. DOI: 10.1021/acscentsci.7b00288.
(5) Li, J.; Fleetwood, J.; Hawley, W. B.; Kays, W. From Materials to Cell: State-of-the-Art and Prospective Technologies for Lithium-Ion Battery Electrode Processing. *Chemical Reviews* **2022**, *122* (1), 903-956. DOI: 10.1021/acs.chemrev.1c00565.
(6) Shea, J.; Huang, X.; Li, M.; Son, S.-B.; Su, C.-C.; Liu, T.; Dong, P.; Chen, A.; Yang, L.; Luo, C.; et al. Impact of Pressure Distribution and Magnitude on the Performance of Lithium Metal Anodes. *Journal of The Electrochemical Society* **2024**, *171* (2), 020528. DOI: 10.1149/1945-7111/ad2648.
(7) Sun, L.; Liu, Y.; Shao, R.; Wu, J.; Jiang, R.; Jin, Z. Recent Progress and Future Perspective on Practical Silicon Anode-based Lithium ion Batteries. *Energy Storage Materials* **2022**, *46*, 482-502. DOI: https://doi.org/10.1016/j.ensm.2022.01.042.
(8) Zhang, Y.; Wu, B.; Mu, G.; Ma, C.; Mu, D.; Wu, F. Recent Progress and Perspectives on Silicon Anode: Synthesis and Prelithiation for LIBs Energy Storage. *Journal of Energy Chemistry* **2022**, *64*, 615-650. DOI: https://doi.org/10.1016/j.jechem.2021.04.013.
(9) Yang, R.; Li, H.; Meng, Q.; Li, W.; Wu, J.; Fang, Y.; Huang, C.; Cao, Y. Influence of PC-based Electrolyte on High-Rate Performance in Li/CrO_x Primary Battery. *Acta Physico Chimica Sinica* **2023**, *0* (0). DOI: 10.3866/pku.Whxb202308053.
(10) Sun, J.; Xu, Y.; Lv, Y.; Zhang, Q.; Zhou, X. Recent Advances in Covalent Organic Framework Electrode Materials for Alkali Metal-Ion Batteries. *CCS Chemistry* **2023**, *5* (6), 1259-1276. DOI: 10.31635/ccschem.023.202302808 (acccessed 2024/12/02).
(11) Zhang, J.; Zhai, Y.; Zhao, Z.; He, J.; Wei, W.; Xiao, J.; Wu, S.; Yang, Q.-H. Research Progress of Functional Binders in Silicon-Based Anodes for Lithium-Ion Batteries. *Acta Physico Chimica Sinica* **2024**, *40* (6), 2306006. DOI: 10.3866/pku.Whxb202306006.
(12) Xie, Y.; Li, M.; Li, J.; Huang, X.; Cai, J.; Yang, Z.; Nguyen, H.; Shaik sulaiman, B. A.; Karami, N.; Chernova, N. A.; et al. Functional Surface Coating to Enhance the Stability of LiNi0.6Mn0.2Co0.2O2. In *Batteries*, 2023; Vol. 9(10), 485.
(13) Li, H.; Li, H.; Yang, Z.; Yang, L.; Gong, J.; Liu, Y.; Wang, G.; Zheng, Z.; Zhong, B.; Song, Y.; et al. SiOx Anode: From Fundamental Mechanism toward Industrial Application. *Small* **2021**, *17* (51), 2102641. DOI: https://doi.org/10.1002/smll.202102641 (acccessed 2024/05/06).

(14) Chen, T.; Wu, J.; Zhang, Q.; Su, X. Recent Advancement of SiOx Based Anodes for Lithium-ion Batteries. *Journal of Power Sources* **2017**, *363*, 126-144. DOI: https://doi.org/10.1016/j.jpowsour.2017.07.073.
(15) Markevich, E.; Salitra, G.; Aurbach, D. Fluoroethylene Carbonate as an Important Component for the Formation of an Effective Solid Electrolyte Interphase on Anodes and Cathodes for Advanced Li-Ion Batteries. *ACS Energy Letters* **2017**, *2* (6), 1337-1345. DOI: 10.1021/acsenergylett.7b00163.
(16) Zhu, Z.; Tang, Y.; Lv, Z.; Wei, J.; Zhang, Y.; Wang, R.; Zhang, W.; Xia, H.; Ge, M.; Chen, X. Fluoroethylene Carbonate Enabling a Robust LiF-rich Solid Electrolyte Interphase to Enhance the Stability of the MoS(2) Anode for Lithium-Ion Storage. *Angew Chem Int Ed Engl* **2018**, *57* (14), 3656-3660. DOI: 10.1002/anie.201712907 From NLM PubMed-not-MEDLINE.
(17) Pritzl, D.; Solchenbach, S.; Wetjen, M.; Gasteiger, H. A. Analysis of Vinylene Carbonate (VC) as Additive in Graphite/LiNi0.5Mn1.5O4Cells. *Journal of The Electrochemical Society* **2017**, *164* (12), A2625-A2635. DOI: 10.1149/2.1441712jes.
(18) Rynearson, L.; Jayawardana, C.; Yeddala, M.; Lucht, B. L. Improved Performance of Silicon-Containing Anodes with Organic Solvent-Solubilized Lithium Nitrate. *Journal of The Electrochemical Society* **2023**, *170* (6). DOI: 10.1149/1945-7111/acdd26.
(19) Kim, K.; Park, I.; Ha, S.-Y.; Kim, Y.; Woo, M.-H.; Jeong, M.-H.; Shin, W. C.; Ue, M.; Hong, S. Y.; Choi, N.-S. Understanding the Thermal Instability of Fluoroethylene Carbonate in LiPF6-based Electrolytes for Lithium ion Batteries. *Electrochim. Acta* **2017**, *225*, 358-368. DOI: https://doi.org/10.1016/j.electacta.2016.12.126.
(20) Hu, Y.-S.; Demir-Cakan, R.; Titirici, M.-M.; Müller, J.-O.; Schlögl, R.; Antonietti, M.; Maier, J. Superior Storage Performance of a Si@SiOx/C Nanocomposite as Anode Material for Lithium-Ion Batteries. *Angewandte Chemie International Edition* **2008**, *47* (9), 1645-1649. DOI: https://doi.org/10.1002/anie.200704287 (acccessed 2024/05/06).
(21) Jin, Y.; Kneusels, N.-J. H.; Marbella, L. E.; Castillo-Martínez, E.; Magusin, P. C. M. M.; Weatherup, R. S.; Jónsson, E.; Liu, T.; Paul, S.; Grey, C. P. Understanding Fluoroethylene Carbonate and Vinylene Carbonate Based Electrolytes for Si Anodes in Lithium Ion Batteries with NMR Spectroscopy. *Journal of the American Chemical Society* **2018**, *140* (31), 9854-9867. DOI: 10.1021/jacs.8b03408.
(22) Hu, M.; Wei, J.; Xing, L.; Zhou, Z. Effect of Lithium Difluoro(oxalate)borate (LiDFOB) Additive on the Performance of High-voltage Lithium-ion Batteries. *Journal of Applied Electrochemistry* **2012**, *42* (5), 291-296. DOI: 10.1007/s10800-012-0398-0.
(23) Dalavi, S.; Guduru, P.; Lucht, B. L. Performance Enhancing Electrolyte Additives for Lithium Ion Batteries with Silicon Anodes. *J. Electrochem. Soc.* **2012**, *159* (5), A642. DOI: 10.1149/2.076205jes.
(24) Xia, L.; Lee, S.; Jiang, Y.; Xia, Y.; Chen, G. Z.; Liu, Z. Fluorinated Electrolytes for Li-Ion Batteries: The Lithium Difluoro(oxalato)borate Additive for Stabilizing the Solid Electrolyte Interphase. *ACS Omega* **2017**, *2* (12), 8741-8750. DOI: 10.1021/acsomega.7b01196 From NLM.
(25) Jagadeesan, S. N.; Barbosa, G. D.; Guo, F.; Zhang, L.; Abeykoon, A. M. M.; Kwon, G.; Olds, D.; Turner, C. H.; Teng, X. Chloride Insertion Enhances the Electrochemical Oxidation of Iron Hydroxide Double-Layer Hydroxide into Oxyhydroxide in Alkaline Iron Batteries. *Chemistry of Materials* **2023**, *35* (16), 6517-6526. DOI: 10.1021/acs.chemmater.3c01496.
(26) Gao, H.; Maglia, F.; Lamp, P.; Amine, K.; Chen, Z. Mechanistic Study of Electrolyte Additives to Stabilize High-Voltage Cathode–Electrolyte Interface in Lithium-Ion Batteries. *ACS Applied Materials & Interfaces* **2017**, *9* (51), 44542-44549. DOI: 10.1021/acsami.7b15395.

(27) Huang, X.; Witherspoon, E.; He, R.; Li, Y.; Yu, J.; Huang, J.; Luo, C.; Li, M.; Liu, T.; Amine, K.; et al. Superior Photodynamic Effect of Single-walled Carbon Nanotubes in Aprotic Media: a Kinetic Study. *Materials Today Energy* **2023**, *32*, 101242. DOI: https://doi.org/10.1016/j.mtener.2022.101242.
(28) Dong, L.; Liang, F.; Wang, D.; Zhu, C.; Liu, J.; Gui, D.; Li, C. Safe Ionic Liquid-sulfolane/LiDFOB Electrolytes for High Voltage $Li_{1.15}(Ni_{0.36}Mn_{0.64})_{0.85}O_2$ Lithium ion Battery at Elevated Temperatures. *Electrochimica Acta* **2018**, *270*, 426-433. DOI: https://doi.org/10.1016/j.electacta.2018.03.108.
(29) Huang, X.; Witherspoon, E.; Li, Y.; Ward, S.; Yu, J.; Wu, H. F.; Ding, H.; Li, Q.; Wang, Z.; Dong, P. Sustainable Generator and In-situ Monitor for Reactive Oxygen Species Using Photodynamic Effect of Single-walled Carbon Nanotubes in Ionic Liquids. *Materials Today Sustainability* **2022**, *19*, 100171. DOI: https://doi.org/10.1016/j.mtsust.2022.100171.
(30) Jiao, S.; Ren, X.; Cao, R.; Engelhard, M. H.; Liu, Y.; Hu, D.; Mei, D.; Zheng, J.; Zhao, W.; Li, Q.; et al. Stable Cycling of High-voltage Lithium Metal Batteries in Ether Electrolytes. *Nature Energy* **2018**, *3* (9), 739-746. DOI: 10.1038/s41560-018-0199-8.
(31) Jurng, S.; Brown, Z. L.; Kim, J.; Lucht, B. L. Effect of Electrolyte on the Nanostructure of the Solid Electrolyte Interphase (SEI) and Performance of Lithium Metal Anodes. *Energy & Environmental Science* **2018**, *11* (9), 2600-2608, 10.1039/C8EE00364E. DOI: 10.1039/C8EE00364E.
(32) Nguyen, C. C.; Lucht, B. L. Comparative Study of Fluoroethylene Carbonate and Vinylene Carbonate for Silicon Anodes in Lithium Ion Batteries. *J. Electrochem. Soc.* **2014**, *161* (12), A1933. DOI: 10.1149/2.0731412jes.
(33) Kim, H. N.; Kim, S. Y.; Ahn, J.; Yim, T. Simultaneous Realization of Multilayer Interphases on a Ni-Rich NCM Cathode and a SiOx Anode by the Combination of Vinylene Carbonate with Lithium Difluoro(oxalato)borate. *ACS Applied Materials & Interfaces* **2024**, *16* (12), 14940-14953. DOI: 10.1021/acsami.4c01032.
(34) Solchenbach, S.; Huang, X.; Pritzl, D.; Landesfeind, J.; Gasteiger, H. A. Monitoring SEI Formation on Graphite Electrodes in Lithium-Ion Cells by Impedance Spectroscopy. *J. Electrochem. Soc.* **2021**, *168* (11), 110503. DOI: 10.1149/1945-7111/ac3158.
(35) Mao, M.; Huang, B.; Li, Q.; Wang, C.; He, Y.-B.; Kang, F. In-situ Construction of Hierarchical Cathode Electrolyte Interphase for High Performance $LiNi_{0.8}Co_{0.1}Mn_{0.1}O_2$/Li Metal Battery. *Nano Energy* **2020**, *78*, 105282. DOI: https://doi.org/10.1016/j.nanoen.2020.105282.
(36) Zhang, W.; Cai, T. H.; Sheldon, B. W. The Impact of Initial SEI Formation Conditions on Strain-Induced Capacity Losses in Silicon Electrodes. *Adv. Energy Mater.* **2019**, *9* (5), 1803066. DOI: https://doi.org/10.1002/aenm.201803066 (acccessed 2024/08/14).
(37) Kim, U.-H.; Kuo, L.-Y.; Kaghazchi, P.; Yoon, C. S.; Sun, Y.-K. Quaternary Layered Ni-Rich NCMA Cathode for Lithium-Ion Batteries. *ACS Energy Letters* **2019**, *4* (2), 576-582. DOI: 10.1021/acsenergylett.8b02499.
(38) Khorsand Zak, A.; Abd. Majid, W. H.; Abrishami, M. E.; Yousefi, R. X-ray Analysis of ZnO Nanoparticles by Williamson–Hall and Size–strain Plot Methods. *Solid State Sciences* **2011**, *13* (1), 251-256. DOI: https://doi.org/10.1016/j.solidstatesciences.2010.11.024.